Underwater Optical Camera Communications based on a Multispectral Camera and Spectral Variations of the LED Emission

Behnaz Majlesein*
Julio Rufo*
jrufo@lightbeecorp.com
LightBee S.L.
Las Palmas de Gran Canaria, Spain

Daniel Moreno
IDeTIC, Universidad de Las Palmas de Gran Canaria
Las Palmas, Spain
dmoreno@idetic.eu

Victor Guerra
IDeTIC, Universidad de Las Palmas de Gran Canaria
Las Palmas, Spain
vguerra@idetic.eu

Jose Rabadan
IDeTIC, Universidad de Las Palmas de Gran Canaria
Las Palmas, Spain
jrabadan@idetic.eu

ABSTRACT

Optical Camera Communication (OCC) applications have intensively used in recent years. Underwater Optical Wireless Communications (UWOC) are one of the most viable alternatives today in underwater environments, compared to traditional acoustic communications or radio communications. UWOC present important and remarkable advantages such as their available bandwidth and the possibility of using COTS devices already present in underwater environments such as LED lighting lamps. This work proposes using a multispectral or hyperspectral camera as an OCC receiver, in short range underwater links, to take advantage of the high spectral resolution of this type of devices regarding conventional cameras. Furthermore, spectral features of the LEDs, usually used as transmitters in OCC, are affected by temperature. Hence, one of the goals of this work is to benefit from those spectral variations that will be grasped by the multispectral camera and thus achieve a new data channel. Therefore, different communication channels could be obtained from a single light source.

CCS CONCEPTS

• **Computer systems organization** → *Embedded systems*; • **Optical Wireless Communications** → *Visible Light Communications*; Optical Camera Communications; • **Networks** → Network reliability.

KEYWORDS

OCC, multispectral, hyperspectral, LED, UWOC

*Authors contributed equally to this research.

1 INTRODUCTION

In the last few years, there has been a rapid rise in the use of Optical Camera Communication (OCC). It is foreseen that significant advancement in this technology will be implemented increasingly soon thanks to the massive presence of optical cameras in consumer electronic devices such as smartphones, tablets and laptops. What is more, OCC has been added as an extension of IEEE 802.15.7 standard on Visible Light Communications (VLC) [1]. This technology used a camera or an image sensor to receive data from a light source. The sensor scanning is based on two different modes. On the one hand, global shutter exposes every pixel per frame simultaneously. Moreover, it can only detect waveforms with bandwidths below half the frame rate. On the other hand, rolling shutter scans the image sequentially. Besides, this mode allows higher speed communication because the optical source's waveform can be captured within a single frame [12]. Nevertheless, the maximum obtainable speed is dependent on the projected size of the light source, as OCC is based on image-forming optics [4]. OCC has been proposed as a suitable technology in applications such as the Internet of Things (IoT), Vehicular Communication, and Indoor Positioning Systems (IPS). Positioning accuracy of OCC-based IPS is within the centimeter range [5, 13], outperforming any RF-based positioning technique. Vehicle-to-Anything (V2X) is another promising application field of OCC due to the uprising presence of vehicle-mounted optical cameras (generally used for surveillance and security).

Underwater Optical Wireless Communications (UWOC) are one of the most viable alternatives today in underwater environments. UWOC, compared to traditional acoustic communications or radio communications, present important and remarkable advantages such as their available bandwidth and the possibility of using COTS devices already present in underwater environments such as LED lighting lamps. The current modulation and coding technologies allow that at a short distance between transmitters and receivers transmission speeds reach values that are not possible in both acoustic and radio communications, very limited in underwater

environments. VLC systems offer a compromise between transmission and link distance compared to other technologies, thus, allow high speeds of short or medium distance transmission.

Apart from this, regarding the camera used as a receiver in OCC, in this technology has been employed several types of cameras such as Single-Lens Reflex (SLR) cameras [6] or smartphones [10]. In all the cases mentioned above, the devices are used to take pictures and videos within the visible range. Their image sensor only permits the capture of RGB images at most, similar to the human eye. However, multispectral cameras (and hyperspectral cameras) can capture a higher number of communication bands than the RGB bands provided by conventional cameras. These have been used in different sectors such as remote sensing [7], agriculture [9] or biotechnology [8]. In this manner, Optical Multispectral Camera Communication (OMCC) would offer a wide range of opportunities.

This work analyzes the LED spectral variations caused by heat and the attenuation due to the underwater channel. The use of a multispectral (or hyperspectral) camera, which has a high spectral resolution, is proposed to take advantage of this typically considered harmful effect. It is expected to get various independent communication channels using a single sort of transmitter, which would lessen the complexity and cost of the system. On the other hand, although this type of camera has a low sampling rate, there are techniques such as spectral signatures extraction to distinguish particular signals at different wavelengths that would improve its performance.

This paper is divided into six sections. Section 2 gives a brief overview of the theoretical background on which the work is based. The characterization methodology and the results concerning the temperature effects on the used LED devices are presented in Sections 3 and 4, respectively. In Section 5, the application of this characterization is proposed using a multispectral camera in an underwater environment. Lastly, some conclusions are drawn in Section 6.

2 LED WAVELENGTH DEPENDENCE ON TEMPERATURE

The working principle of LED is spontaneous emission of light. That light is emitted when an electron obtains enough energy to traverse the forbidden energy gap of the semiconductor. Then, a photon is emitted when that electron goes back to a lower energy level. The emitted photon has a wavelength that is related to the energy gap by Equation 1. In addition, the energy gap is affected by the p-n junction temperature, depending on the LED's substrate, which is usually modeled using Equation 2. According to [11], in most semiconductor materials energy gap diminishes as temperature increases. Therefore, as wavelength is inversely proportional to energy gap (Equation 1), the peak wavelength of the LED grows with temperature.

$$E_g = hf = \frac{hc}{\lambda} \tag{1}$$

$$E_g = E_0 - \frac{\alpha T^2}{T + \beta} \tag{2}$$

where h is Planck constant, f is frequency, c is the speed of light in vacuum and λ is wavelength. T is temperature, E_0 is energy gap at 0

temperature condition, and α and β are semiconductor-dependent constants, which are empirically determined[11].

However, the metallic content in the LED material must be considered. For instance, [14] proved that the band gap might not follow the decrement as the LED heats up, but it may increase with temperature depending on Indium (In) content in InGaN alloys (green and blue LEDs).

Apart from this, spectral width and luminous efficiency are affected by temperature as well. Normally, the conversion efficiency decreases and the spectral width increases as temperature grows [3]. Based on this, it is intended to use a high spectral resolution camera, such as a multispectral camera, to check if these slight wavelength changes in the LED emission are detectable by it. Then, grasping these generally undesired variations, this work proposes improving communications by increasing the number of communication channels.
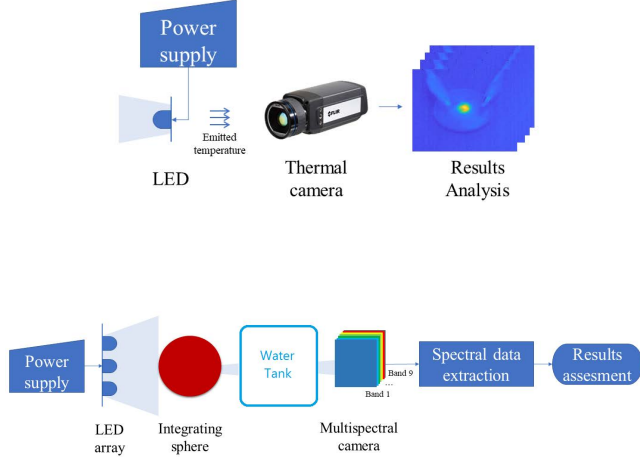
3 METHODOLOGY

The primary goal of this work is to benefit from the spectral variations that temperature effects on LEDs, so that a multispectral camera detects those changes and finally use it for OCC purposes. To accomplish this objective, RGB LEDs have been characterized by focusing on the effect of temperature on their emitted spectrum. Moreover, a multispectral camera has been used to set a communication link with those LEDs as transmitters in an underwater environment. Lastly, spectral responses of the emitters have been extracted from the pictures to evaluate the practicability of Optical Multispectral Camera Communications (OMCC) and the use of the LED wavelength variations induced by temperature.

The LEDs under study (common cathode RGB LED with no heat sinks) were driven using currents ranging from 10 mA to 130 mA by an Ethernet-controlled current source to induce them different junction temperatures. Additionally, the temperature was previously stabilized for 5 minutes. This experimental characterization consisted of three different processes. Firstly, the junction temperature of the LEDs has been measured by a thermal imaging camera, as shown in Fig. 1 (top). The employed camera was a FLIR A645, whose main features are a pixel resolution of 640 x 480 and a high sensitivity below 50m. For each current, the maximum temperature of the LED has been recorded.

Secondly, a spectrometer (Spectral Products SM442) has been used to obtain wavelength data of the LED in the visible range. Due to the high intensity of the LED beam, a 15-centimeters ABS-plastic cylinder has been used to distance the LED from the light input, allowing to receive the signal within the dynamic range of the spectrometer. This fix does not affect the measurement, because of the spectrometer is only needed to get the wavelength information of the LED and visualize shape variations (not absolute changes). Finally, the spectral radiant power of the LED in the visible spectral range has been measured using an integrating sphere and a light meter (Gigahertz BTS256). This device also permits to acquire spectral information; however, the spectrometer provided a better spectral resolution (1 nm vs. 5 nm).

After the LEDs' characterization, the aim was to capture the wavelength variation in the LEDs by a camera. It was needed to have a high spectral resolution camera that can detect the slight

phenomena are used to characterize the extinction coefficient $c(\lambda)$ at a wavelength determined by equation 3.

$$c(\lambda) = \alpha(\lambda) + \beta(\lambda) \tag{3}$$

where $\alpha(\lambda)$ represents the absorption coefficient and $\beta(\lambda)$ represents the total dispersion coefficient. To calculate the minimum necessary power in an underwater link to induce a detectable signal, assuming no misalignment between both endpoints, we can use Equation 4.
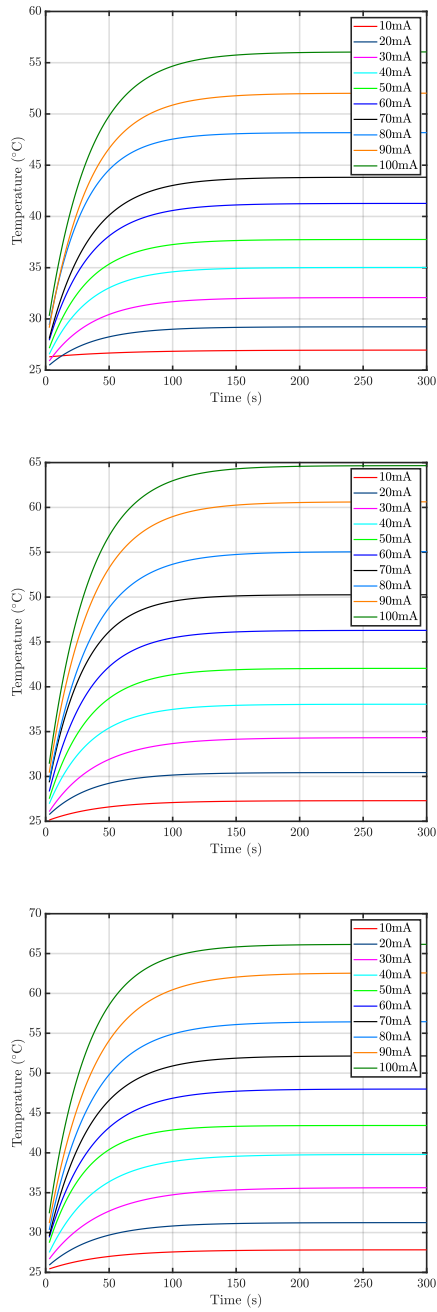
$$P_{tx,min} = \frac{S_{rx} \cdot d^2}{A_{eff} \cdot e^{-c(\lambda)d} \cdot R(\theta, \phi)} \tag{4}$$

where S_{rx} is the receiver's sensitivity, A_{eff} is the effective receiver area, d is the link range, $R(\theta, \phi)$ is a factor that depends on the type of source and its orientation, and $e^{-c(\lambda)d}$ is a coefficient that models the effect of extinction phenomena that occur in the underwater environment[2]. For this work, only clear tap water was used.

Then, the multispectral camera receives that beam and a picture is taken. The camera parameters were adjusted so that the acquired image would not be saturated. The pictures have been saved as single-band images in ENVI file format, which includes one header and one file with multispectral data. Finally, the pictures were cropped selecting only the part that contains the emitted light and from these, the spectral signatures were extracted. With the spectral response of the LED at various temperatures, an evaluation can be made of how well the several signals are distinguished by the camera.

## 4 CHARACTERIZATION RESULTS

In Fig. 2, some examples of the temperature-time behavior of the RGB LEDs are presented. It depicts an exponential growth which is higher as the driving current increases. Interesting information can be extracted from these graphs, such as that the highest temperature was obtained on the blue LED, followed by the green and the red LEDs. It also can be seen that at 10 mA the temperature kept almost constant. As an example, Fig. 3 shows several thermal pictures of the red LED at low and high temperatures. Fig. 4 (top) shows the effects of the induced high temperature on the LED emission, by increasing the polarization current, on the peak wavelengths of each RGB color. Table 1 details the spectral information in Fig. 4 (top) showing the peak wavelengths and the Full Width at Half Maximum (FWHM) values of each spectrum. It can be seen that by rising the temperature the emitted wavelength grew as expected and, consequently, the peak wavelength shifted. The largest shift was obtained in the red LED with a difference of 21.1 nm between the minimum and the maximum temperature (peak wavelength at 659.6 nm at 27 and 680.7 nm at 65). It was followed by a 13.5 nm shift in blue (from 486.1 nm at 28 to 499.6 nm at 78). In green, the peak wavelength did not increase with temperature in the same way that red and blue did. In this case, the highest peak wavelength was found at the minimum temperature (547.2 nm, 27). The green source color of the employed LED is made with InGaN on Silicon (Si). As seen in Section 2, In content in this alloy can affect in such a way that when the temperature increases the energy gap also grows, so wavelength decreases. In addition to the peak wavelength

Figure 1: System setup schemes. Scheme used to get the temperature data (top) and scheme used to get the spectral data (bottom).

variations due to temperature; in this case, a multispectral camera, in order to reach this objective. Specifically, the multispectral camera used was the CMS-C1-C-EVR1M-GigE by SILIOS Technologies. It is a 9-bands camera (8 color narrow bands and 1 panchromatic band) that covers the wavelength range from 400 to 1000 nm. It has a CMOS sensor and a resolution of 1280 (H) x 1024 (V) in the raw picture and 426 (H) x 339 (V) in the spectral pictures.

Fig. 1 (bottom) depicts the scheme followed to collect the spectral information of the LED using the multispectral camera. The light beam of these LEDs passes through an integrating sphere that concentrates it on a narrow point. Then the light goes through a water tank that can easy simulate an underwater channel. One of the main characteristics of the underwater channel in terms of its response in wavelength is its low coherence time, that is, the intervals where the channel can be considered quasi-stationary are very small. This renders the linear and temporally invariant channel approximations invalid a priori, as demonstrated in [2]. It should be noted that this is not the same throughout the ocean, since it only occurs in areas where drastic changes in temperature and salinity occur and large amounts of marine particles are concentrated. In other areas such as the seabed, this statement would not be true, since in that case the temperature is uniform and there is hardly any movement, so the channel could be considered quasi-stationary. On the other hand, the interaction between light, water molecules and underwater particles gives rise to two wavelength-dependent effects that involve attenuation of the optical signal: spatial scattering and energy absorption. The main cause of the absorption of light in water is the excitation of the vibration state of water molecules by photons and other dissolved particles. On the other hand, light scattering refers to processes in which the direction of the photon is changed and can take place both in molecules or in dissolved particles. In this way, the absorption and scattering

Figure 2: Temperature behavior of the RGB LED: Red (top), green (middle) and blue (bottom).

shift, it is noteworthy how the width changed with the temperature variation. The most striking change was acquired in blue, having a difference between the width at 28 and 66 of roughly 30 nm. Note that the intensity values were normalized in Fig. 4 (top) because the approach was to analyze only the spectral information.

Fig. 4 (bottom) reports the spectral radiant power of the LED in W/nm. The highest levels were obtained for the blue LED, followed by green and red. It can be noted that at the maximum temperature, when the LED is supplied with 130 mA, the power decreased with respect to the second maximum. As a consequence of that, temperature expectedly affected the efficiency of the LED. Furthermore, it shows the wavelength variations, as well as the FWHM changes on temperatures.
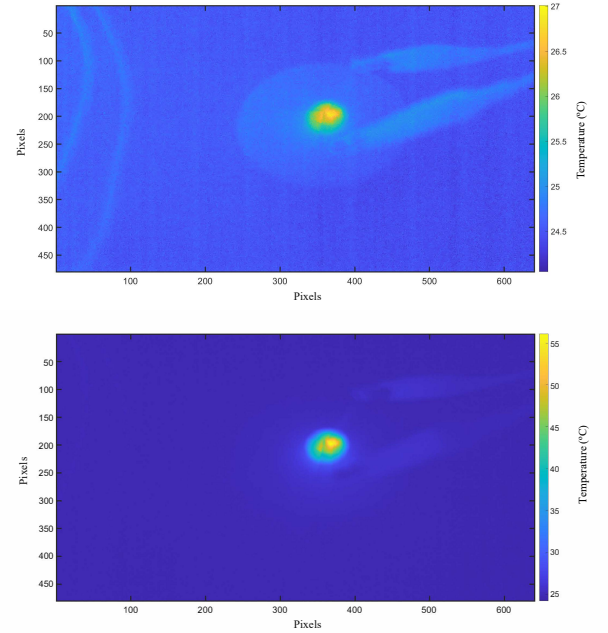

Figure 3: Examples of images of the red LED driven at different currents, taken by a thermographic camera. LED at 10 mA (top) and LED at 100 mA (bottom).

Table 1: Spectral information at different temperatures.

LED	Red			
Current (mA)	10 (27)	50 (38)	100 (56)	130 (65)
Peak wavelength (nm)	659.6	663.6	672.5	680.7
FWHM (nm)	8.73	14.97	22.33	24.15

LED	Green			
Current (mA)	10 (27)	50 (42)	100 (65)	130 (76)
Peak wavelength (nm)	547.2	544.9	545.1	546.8
FWHM (nm)	23.73	31.80	40.92	43.18

LED	Blue			
Current (mA)	10 (28)	50 (43)	100 (66)	130 (78)
Peak wavelength (nm)	486.1	486.1	490.5	499.6
FWHM (nm)	16.68	29.62	45.85	32.10
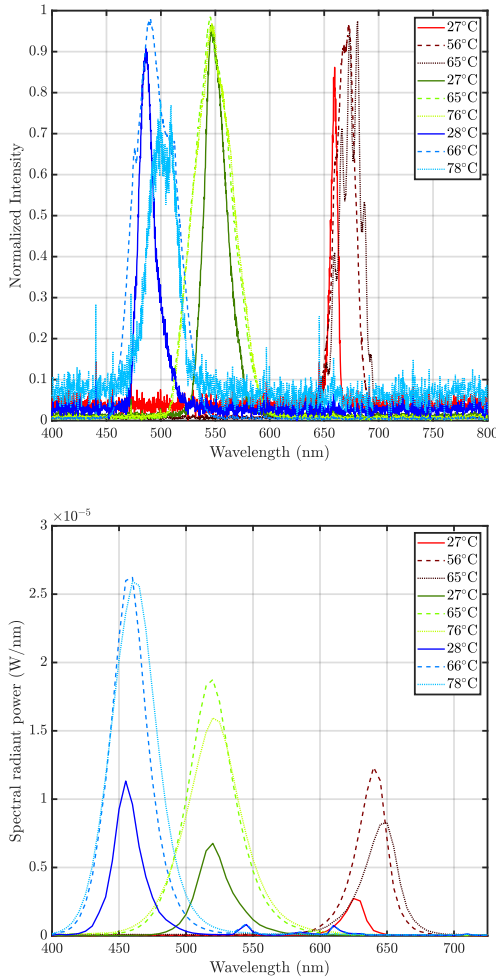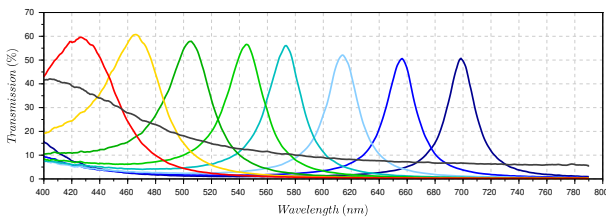
5 MULTISPECTRAL CAMERA RESULTS

The images captured by the camera show the spectral variations caused by changing the LED junction temperature. Those changes can be observed in the spectral signatures of the LED shown in Fig. 6. As a case in point, Fig. 6 (bottom) depicts the several levels of energy of the blue LED, supplied with various currents (therefore, at different temperatures), with respect to the 9 bands of the multispectral camera. Targeting the bands 1, 2 and 3, centered in 427, 461 and 501 nm, respectively, as the analyzed results were obtained on the blue LED, there are some phenomena to consider. Besides, a high level is placed in band 9, which corresponds to the panchromatic band. However, the focus is not in this band, because the only remarkable consequence is the increase in level due to the increment in current. Firstly, part of the energy captured in the band 1 was captured in the band 2 as temperature grew, causing an increment in the level of this band. The identical happened with bands 2 and 3. It occurred because the peak wavelength of the LED gradually shifted, so the bands 2 and 3, which have an FWHM of the order of 50 nm (see Fig. 5), took more information. Additionally, it is perceptible a growth in level as expected, since the way chosen to raise the temperature is by increasing the driving current, ergo the power of the LED also increases. Figs. 6 (top) and 6 (bottom) depict the spectral signatures of the red and green LED, respectively, showing similar results. These results suggested that several communication channels can be obtained from a single emission source since the slight changes in wavelength are detected by the multispectral camera.
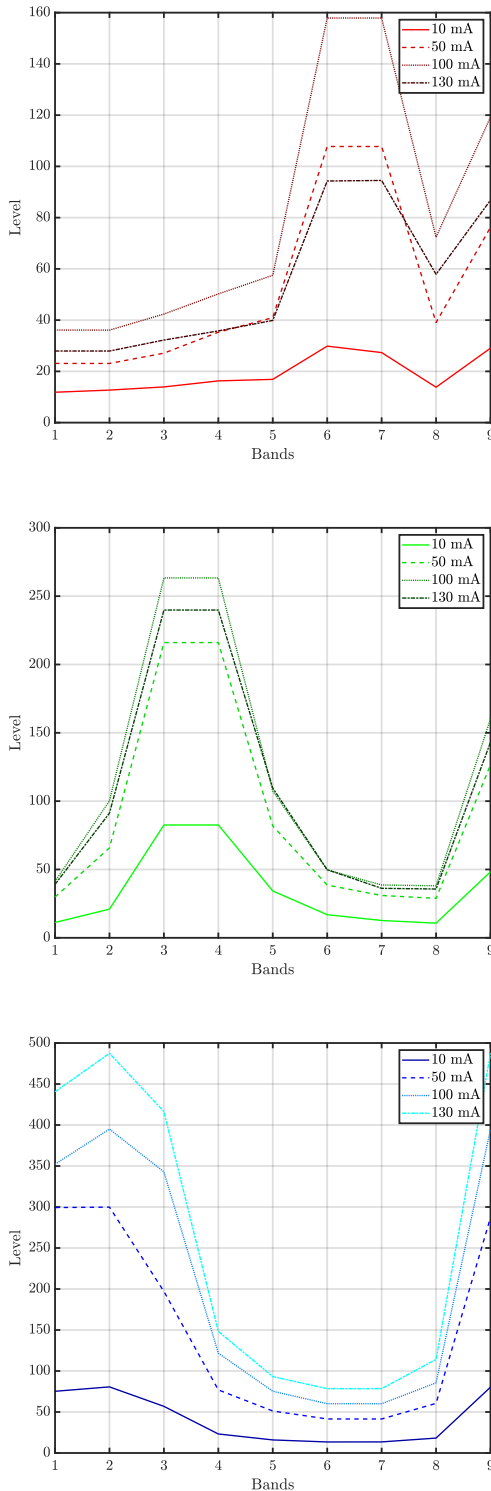
6 CONCLUSIONS

In this work, several RGB LEDs have been characterized, especially to visualize the effect of the transmitter's temperature in the wavelength/spectrum of the emitted light. Furthermore, it has been utilized a multispectral camera taking pictures of the light beam of the LED and analyzing those wavelength variations. The spectral response of the RGB LEDs has been extracted and how the wavelength shifts have been checked. Therefore, as the spectral changes in the emitted light can be observed by using a multispectral camera, it takes advantage of that phenomenon considered harmful. So, the more variation in the peak wavelength of the LED is affected by temperature, the better. Thus, this paper proposes to use those dissimilarities to create separable communication channels in an OMCC application.

This led us to conclude that employing, for instance, two receivers with two different optical filters, will be feasible to separate each signal by using the same transmitter device. Using the temperature to tune the wavelength of the LED will allow this to be done. It will also be possible to use a camera with enough spectral resolution, such as a multispectral or a hyperspectral camera, which captures the light beam in its several bands with greater or lesser intensity depending on the wavelength shift.

The evidence of this work points towards the idea that temperature effects in emitters, usually considered detrimental, can be detected by high-spectral-resolution cameras and used for applications such as Wavelength Division Multiplexing (WDM) (Fig. 7).In this case, the results of this study indicated that the red LED got more spectral variations than green and blue.

Figure 4: Characterization of the RGB LED at different temperatures: Normalized RGB LED spectra (top) and spectral radiant power (bottom). Solid line, dashed line, dotted line and dash-dot line correspond to 10 mA, 50 mA, 100 mA and 130 mA, respectively.

Figure 5: Filter specifications.
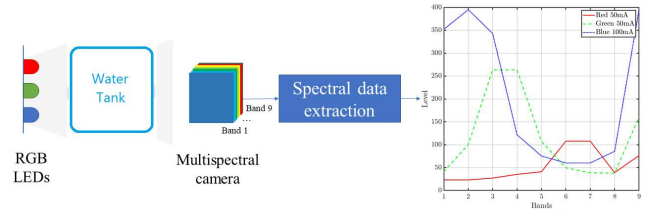
Figure 7: This figure is an example of a proposed diagram for WDM. By sending three different color signals that are captured by the multispectral camera, after extracting their spectral signatures, each signal could be separated.

ACKNOWLEDGMENTS

REFERENCES

[1] April 2019. Short-Range Optical Wireless Communications (802.15.7-2018).
[2] L. Mullen B. Cochenour and A. Laux. 2008. Characterization of the beam-spread function for underwater wireless optical communications links. *OCEANS engineering* 33, 3 (01 Mar 2008), 311–335. https://doi.org/10.1023/A:1008889222784
[3] Jeong Park and C. C. Lee. 2005. An electrical model with junction temperature for light-emitting diodes and the impact on conversion efficiency. *IEEE Electron Device Letters* 26, 5 (May 2005), 308–310. https://doi.org/10.1109/LED.2005.847407
[4] Cristo Jurado-Verdu, Vicente Matus, Jose Rabadan, Victor Guerra, and Rafael Perez-Jimenez. 2019. Correlation-based receiver for optical camera communications. *Opt. Express* 27, 14 (Jul 2019), 19150–19155. https://doi.org/10.1364/OE.27.019150
[5] Y. Li, Z. Ghassemlooy, X. Tang, B. Lin, and Y. Zhang. 2018. A VLC Smartphone Camera Based Indoor Positioning System. *IEEE Photonics Technology Letters* 30, 13 (July 2018), 1171–1174. https://doi.org/10.1109/LPT.2018.2834930
[6] Pengfei Luo, Min Zhang, Zabih Ghassemlooy, Hoa Le Minh, Hsin-Mu Tsai, Xuan Tang, and Dahai Han. 2015. Experimental demonstration of a 1024-QAM optical camera communication system. *IEEE photonics technology letters* 28, 2 (2015), 139–142.
[7] Javier Marcello, Dionisio Rodriguez-Esparragon, and Daniel Moreno. 2018. Comparison of land cover maps using high resolution multispectral and hyperspectral imagery. In *IGARSS 2018-2018 IEEE International Geoscience and Remote Sensing Symposium*. IEEE, 7312–7315.
[8] F. Meriaudeau, V. Paquit, N. Walter, J. Price, and K. Tobin. 2009. 3D and multispectral imaging for subcutaneous veins detection. In *2009 16th IEEE International Conference on Image Processing (ICIP)*. 2857–2860. https://doi.org/10.1109/ICIP.2009.5414511
[9] M. Rosenberger. 2014. Multispectral edge detection algorithms for industrial inspection tasks. In *2014 IEEE International Conference on Imaging Systems and Techniques (IST) Proceedings*. 232–236. https://doi.org/10.1109/IST.2014.6958479
[10] Shivani Rajendra Teli, Stanislav Zvanovec, and Zabih Ghassemlooy. 2019. The first tests of smartphone camera exposure effect on optical camera communication links. In *2019 15th International Conference on Telecommunications (ConTEL)*. IEEE, 1–6.
[11] Yatendra Pal Varshni. 1967. Temperature dependence of the energy gap in semiconductors. *physica* 34, 1 (1967), 149–154.
[12] Zhaocheng Wang, Qi Wang, Wei Huang, and Zhengyuan Xu. 2017. *Visible light communications: Modulation and signal processing*. John Wiley & Sons.
[13] J. Xu, C. Gong, and Z. Xu. 2018. Experimental Indoor Visible Light Positioning Systems With Centimeter Accuracy Based on a Commercial Smartphone Camera. *IEEE Photonics Journal* 10, 6 (Dec 2018), 1–17. https://doi.org/10.1109/JPHOT.2018.2878532
[14] ChuanZhen Zhao, Rong Zhang, Bin Liu, DeYi Fu, Hui Chen, Ming Li, ZiLi Xie, XiangQian Xiu, ShuLin Gu, and YouDou Zheng. 2012. The temperature dependence of optical properties of InGaN alloys. *Science China Physics, Mechanics and Astronomy* 55, 3 (2012), 396–399.

Figure 6: Spectral signatures of the RGB LED at different temperatures: Red (top), green (middle) and blue (bottom). Solid line, dashed line, dotted line and dash-dot line correspond to 10 mA, 50 mA, 100 mA and 130 mA, respectively.